J Solid State Electrochem (2004) 8: 908–913
DOI 10.1007/s10008-004-0498-9

ORIGINAL PAPER

Heon-Cheol Shin · Meilin Liu · B. Sadanadan
Apparao M. Rao

Lithium insertion into chemically etched multi-walled carbon nanotubes

Received: 12 May 2003 / Accepted: 24 December 2003 / Published online: 5 March 2004

Abstract Lithium insertion (deinsertion) into (from) chemically etched multi-walled carbon nanotubes (c-MWNTs) has been investigated using various electrochemical techniques such as chronopotentiometry, chronoamperometry, and electrochemical impedance spectroscopy. The results indicate that not only the reversible capacity but also the rate capability was improved by a chemical etching (shortening) of the nanotubes. The observed enhancement in capability at high-rate lithium insertion/deinsertion is attributed to the increased electrochemically active area and reduced lithium diffusion length along the nanotubes, resulting from the structural defects and open ends of the c-MWNTs.

Keywords Carbon nanotube · Chemical etching · Lithium battery · Rate capability

Introduction

Nano-structured materials for energy storage have attracted much attention recently because of their potential to offer high energy and power density and long cycle life. Among them, carbon nanotubes have been widely studied as electrodes for lithium batteries since their one-dimensional structure with a central core in multi-walled carbon nanotubes (MWNTs) or interstitial channels in single-walled carbon nanotube (SWNT) bundles may allow rapid insertion/deinsertion of lithium into/from the nanotubes [1, 2, 3, 4, 5, 6, 7, 8, 9, 10, 11]. While some have questioned the feasibility of using carbon nanotubes for anodes in practical lithium batteries in their pure, as-prepared forms [1, 2], a variety of chemically and mechanically modified carbon nanotubes are being prepared to improve their electrochemical properties for lithium storage [4, 7, 8, 9, 10, 11].

Today, bulk quantities of high purity MWNTs can be readily produced cost effectively through catalytic decomposition of ferrocene and xylene under atmospheric pressure at moderate temperatures on bare quartz substrates [12]. While it was demonstrated that the as-prepared MWNTs (a-MWNTs) created by the catalytic process have great potential to be used for an anode material in lithium batteries since they show excellent cyclability as well as very small hysteresis during lithium insertion/deinsertion [13], the reversible specific capacity and rate capability must be significantly improved for practical use.

Recently, a chemical etching process has been employed to reduce the actual diffusion length of lithium through the SWNTs and it has been suggested that the etched (i.e. shortened) SWNT shows considerably better performance for lithium storage than the as-prepared nanotube [8, 9]. On the other hand, from a systematic study on the electrochemical lithium insertion into a capped (closed) MWNT, Maurin et al. [14] have reported a heterogeneous swelling of the nanotubes during lithiation, indicating that the lithium transport through the MWNT is not a simple one-dimensional diffusion process. In this case, the preferential sites for lithium insertion into the MWNT are most likely the lateral defects on the sidewalls, as predicted by recent ab initio analyses [15, 16]. This implies that the electrochemical performance of the MWNT would be much improved for the modified nanotubes with higher lateral defects and open ends because of the increased active sites for electrochemical lithium insertion/deinsertion. Here, we report our initial results on chemically etched MWNTs (c-MWNTs) in an effort to shorten the lithium diffusion length in the solid state and to increase the electro-

H.-C. Shin · M. Liu (✉)
School of Materials Science and Engineering,
Georgia Institute of Technology, Atlanta,
GA 30332-0245, USA
E-mail: meilin.liu@mse.gatech.edu
Tel.: +1-404-8946114
Fax: +1-404-8949140

B. Sadanadan · A. M. Rao
Kinard Laboratory of Physics, Clemson University,
Clemson, SC 29634, USA

chemically active area. The electrochemical properties of both as-prepared MWNT and chemically shortened MWNT are presented, including the reversible capacity, cyclability, and rate capability.

Experimental

Specimen preparation

High-purity multi-walled carbon nanotube samples were prepared through catalytic decomposition of a ferrocene-xylene mixture, as described elsewhere [12, 13]. In order to prepare shortened nanotubes, the a-MWNTs (500 mg) were sonicated at room temperature in 50 mL oleum [conc. $H_2SO_4 + 30\%$ fuming SO_3 (Aldrich)] for 24 h. The suspension was then vigorously centrifuged to recover the MWNTs, followed by washing repeatedly with deionized water and acetone and then drying under vacuum. A drop of the suspension containing c-MWNTs dispersed ultrasonically in tetrahydrofuran (THF) was placed on a transmission electron microscope (TEM) grid and subsequently analyzed using a TEM.

Electrochemical test

A three-electrode electrochemical cell was employed for all electrochemical measurements, using lithium foils as the counter and reference electrodes. The working electrode was composed of a-MWNTs or c-MWNTs (85 wt%), carbon black (5 wt%), and poly(vinylidene fluoride) (PVDF) binder (10 wt%). The slurry of the mixture was cast on a Ni plate, followed by drying at 180 °C in vacuum for 24 h and uniaxial pressing between two flat stainless steel plates at ~500 psi for 5 min.

A Celgard 2500 separator, wetted with 1 M solution of $LiPF_6$ in a 50/50 (v/v) mixture of ethylene carbonate (EC) and diethyl carbonate (DEC), was sandwiched between an a-MWNT or c-MWNT working electrode and a lithium counter electrode. Both the galvanostatic and potentiostatic experiments were performed using a Solartron 1285 potentiostat. The impedances were typically measured in the frequency range from 10 mHz to 100 kHz using an EG&lock-in amplifier (model 5210) in combination with an EG&G potentiostat/galvanostat (model 273A) interfaced with a computer. All cells were assembled and tested in a glove box (Vacuum Atmospheres) filled with purified argon gas.

Results and discussion

Microstructure and morphology

Shown in Fig. 1a is a typical TEM image of c-MWNTs, from which the length of the tubes was estimated and the number of tubes as a function of length is plotted in Fig. 1b. From the length distribution plot it is evident that the majority of chopped tubes (~45%) are in the range of 200–400 nm in length. The TEM image of a-MWNTs reveals that the average length of the unchopped tubes is in the range 10–30 μm [12], about two orders of magnitude longer than the chopped ones.

In order to explore the structural changes of MWNTs caused by the chemical etching process, high-resolution TEM images were taken before (a-MWNT, Fig. 2a) and after the sonication process (c-MWNT, Fig. 2b). Unchopped MWNT is characterized by inner graphene layers, i.e. a nanotube, and a very thin outer disordered

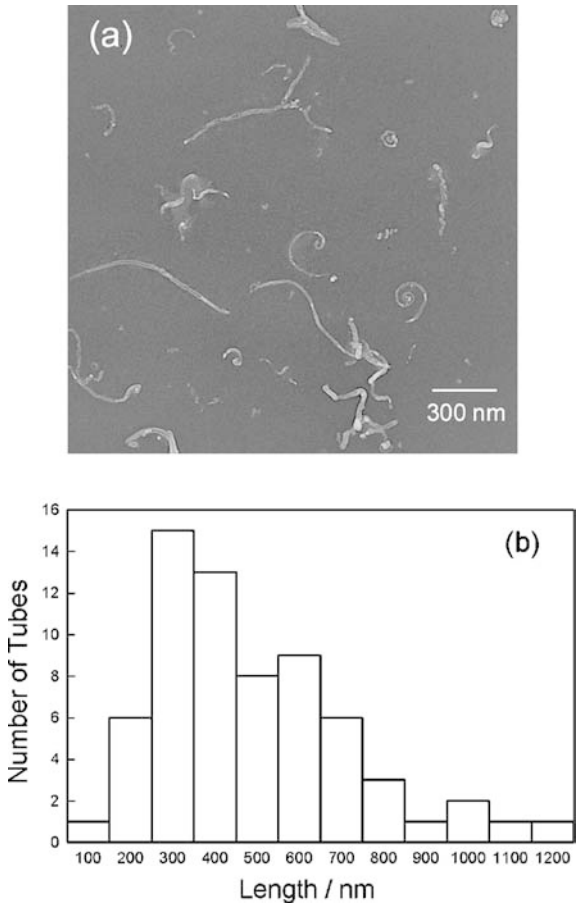

Fig. 1 (**a**) Typical TEM image and (**b**) approximate length distribution of the chemically etched nanotubes (c-MWNTs)

phase which covers the inner nanotube uniformly. On the other hand, the walls of the nanotube have been seriously damaged after the sonication process, resulting in lots of defects, edge sites, and/or kinks in the graphene sheets of the nanotube (Fig. 2b). This is consistent with a previous report where the sonication of MWNTs was proved to mechanically damage the sides of the nanotubes [17]. From the high-resolution TEM images of the c-MWNTs, it is likely that the various shapes of the c-MWNTs, such as straight, round, and/or spiral, etc., shown in Fig. 1a, are attributed to the non-uniform destruction of the outer walls during the chemical etching.

Recent ab initio studies on lithium insertion into carbon nanotube systems [15, 16] suggested that lithium transport through the sidewall or capped zone of a closed tube is energetically unfavorable; however, lithium ions can enter tubes through structural defects on the sidewalls or through the open ends of the nanotube. Accordingly, it is expected that c-MWNTs have much better kinetic properties as compared to a-MWNTs, primarily due to an increase in the electrochemically active surface area (i.e. the available sites for lithium insertion) originating from the open ends of short fragmented nanotubes and the large amount of structural defects on their surface.

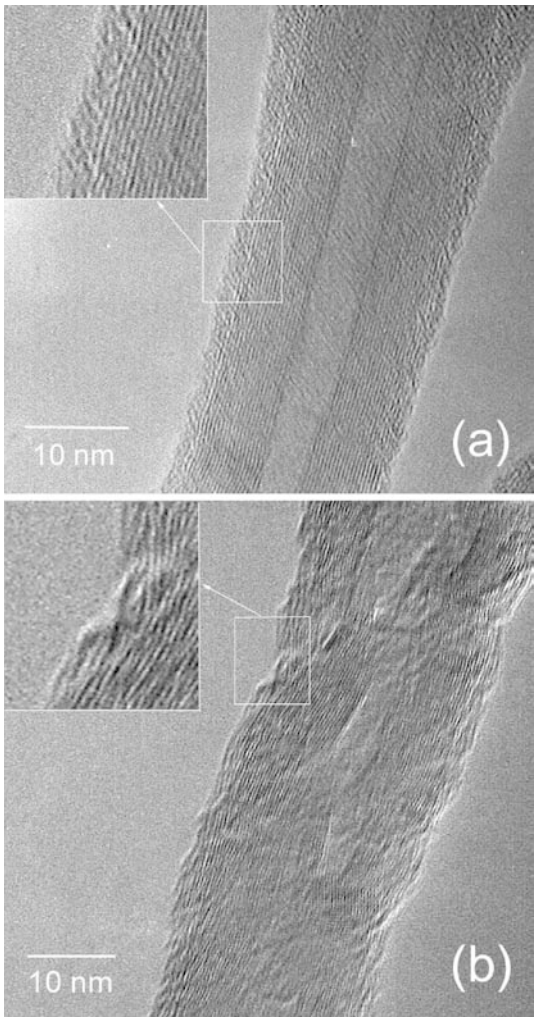

Fig. 2 Typical high-resolution TEM images of (**a**) an as-prepared nanotube (a-MWNT) and (**b**) a c-MWNT

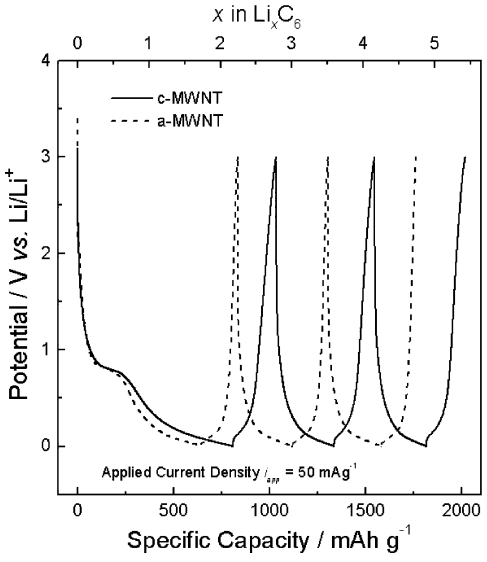

Fig. 3 Voltage profiles for the first three cycles obtained from a-MWNTs (*dashed line*) and c-MWNTs (*solid line*) in a 1 M $LiPF_6$-EC/DEC solution at a current density of 50 mA g^{-1} carbon nanotubes

Lithium insertion/deinsertion behavior: voltage profiles and cyclability

Shown in Fig. 3 are the voltage profiles of a-MWNT/Li (dotted lines) and c-MWNT/Li cells (solid lines) at a current density of 50 mA g^{-1} MWNTs for the first three cycles. For both a-MWNT and c-MWNT there is large irreversible capacity for the first lithium insertion cycle caused by decomposition of the electrolyte and the formation of a solid electrolyte interphase layer at ca. 0.8 V (vs. Li/Li^+) [18]. In subsequent cycles, however, lithium deinsertion (insertion) from (into) the nanotubes is nearly reversible. The performance of a-MWNTs and c-MWNTs is summarized in Table 1, along with the corresponding values for a variety of carbonaceous materials for the sake of comparison.

As shown in Table 1, the irreversible capacity of c-MWNTs ($C_{ins}-C_{de}=586$ mA h g^{-1}) for the first cycle is about 30% larger than that of a-MWNTs (455 mA h g^{-1}). It is generally accepted that irreversible capacity of carbonaceous materials at the first cycle is largely attributed to electrolyte instability, i.e. decomposition of the electrolyte on the electrode surface and reaction of lithium with active sites (such as OH and carbon radicals) in the bulk electrode, which are typically enhanced with increasing surface area and degree of disorder in the carbonaceous materials, respectively [19]. Accordingly, the increase in the irreversible capacity of the c-MWNTs is due probably to increased surface area and structural defects/disordered phase of the c-MWNTs induced by the chemical etching process, as seen in Fig. 2b.

On the other hand, the reversible capacity of c-MWNTs (223 mA h g^{-1}) at a lithium deinsertion rate of 50 mA g^{-1} increased by about 20% as compared to that of a-MWNTs (189 mA h g^{-1}). This indicates that the chemical etching process is useful to generate the active sites available for reversible lithium storage, consistent with the previous reports on the enhanced lithium storage for mechanically/chemically modified carbonaceous materials [4, 8, 9, 20, 21, 22]. However, a larger irreversible capacity and a smaller reversible capacity of c-MWNTs than those of graphites, as seen in Table 1, make it still impractical as an electrode material in lithium batteries. In this respect, recent publications reporting a small initial capacity loss (142 mA h g^{-1}) [7] and a large reversible capacity (640 mA h g^{-1}) [3] might give us a clue for improving further the lithium storage characteristics of the present MWNTs. This includes structural modification of MWNTs by doping [7] or chemical/mechanical treatment to introduce additional active sites [4, 8, 9].

Shown in Fig. 4 are the second-cycle voltage profiles of an a-MWNT/Li cell (dotted line) and a c-MWNT/Li cell (solid line) at a current density of 50 mA g^{-1} carbon

Table 1 Performance of various carbonaceous materials

Material[a]	1st Li insertion, C_{ins} (mA h g^{-1})	1st Li deinsertion, C_{de} (mA h g^{-1}) (rate/mA g^{-1})	Efficiency, C_{de}/C_{ins}	Li deinsertion rate (mA g^{-1}) (capacity retention/mA h g^{-1})
a-MWNT	644	189 (50)	0.29	50 (176); 80 (159);120 (135); 150 (108)
c-MWNT	809	223 (50)	0.28	50 (189); 80 (174); 120 (156); 150 (143)
MWNT1	1540	640 (20)	0.42	20 (520); 40 (420); 60 (360); 80 (320)
MWNT2	1157	282 (20)	0.24	20 (270); 40 (225); 60 (200); 80 (185)
MWNT3	850	320[b] (10)	–	10(340[b]); 25(250[b]); 60 (120[b]); 100 (90[b])
MWNT4	322	180 (50)	0.60	20 (200); 30 (190); 50 (180)
SWNT1	1660	460 (20)	0.28	20 (460); 186 (405)
SWNT2	–	698 (50)	–	–
Graphite1	397	330 (43)	0.83	43 (300); 93 (240); 149 (170)
Graphite2	493	371 (43)	0.75	43 (370); 93 (360); 149 (350)

[a]a-, c-MWNT: this work; MWNT1: pyrolysis of acetylene, slightly graphitized MWNT [3]; MWNT2: pyrolysis of ethylene, well-graphitized MWNT [3]; MWNT3: chemical vapor deposition [23]; MWNT4: graphite arc technique, B-doped MWNT [7]; SWNT1: dual pulsed laser vaporization, purified SWNT [5, 6]; SWNT2: laser ablation method, chemically etched SWNT [8, 9]; graphite1: natural graphite [26]; graphite2: jet-milled graphite [26]
[b]Capacity for lithium insertion

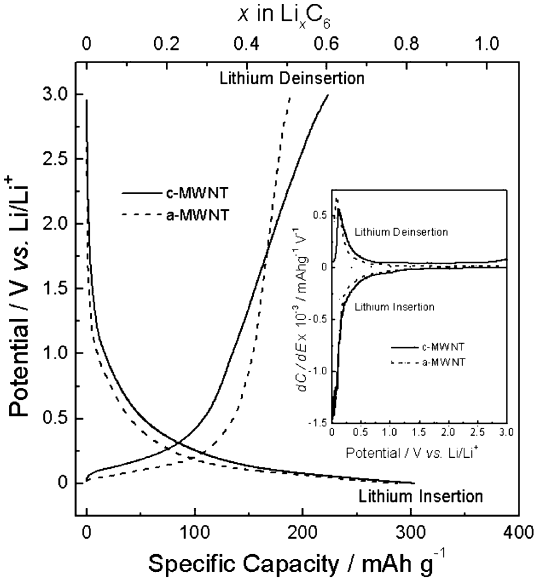

Fig. 4 Voltage profiles for the second cycle obtained from a-MWNTs (*dashed line*) and c-MWNTs (*solid line*). *Inset* is the dependence of differential capacity on voltage, reconstructed from the voltage profiles

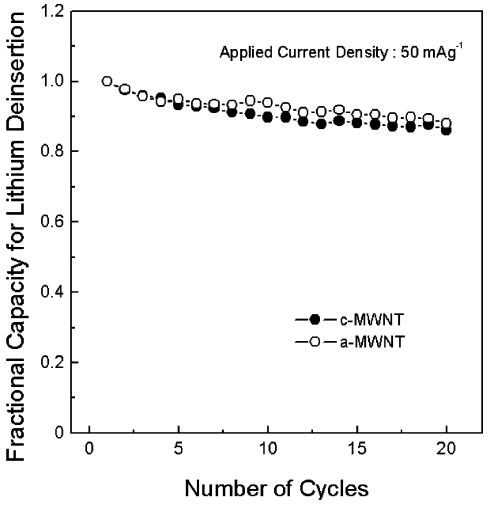

Fig. 5 Variation of fractional capacity for lithium deinsertion from a-MWNTs (*open circles*) and c-MWNTs (*solid circles*) with the number of cycles at a constant current of 50 mA g^{-1} carbon nanotubes

nanotubes. It is noted that the concavity of the curve for the c-MWNTs is lower than that for the a-MWNTs. In other words, lithium intercalates into or deintercalates from the c-MWNTs at higher potential as compared to the a-MWNTs below 1.5 V (vs. Li/Li^+). In order to describe effectively the lithium insertion/deinsertion behavior, we reconstructed the differential specific capacities (d C/d E) versus cell voltages in the inset of Fig. 4. Both the differential capacity curves obtained from the a-MWNTs (dotted lines) and c-MWNTs (solid lines) were well characterized by a high absolute value of d C/d E below 0.5 V (vs. Li/Li^+), an indication of lithiation/delithiation in a very narrow potential window. Nevertheless, it is noted that the maximum absolute values of d C/d E in c-MWNTs, especially the differential capacity curve for lithium deinsertion, are somewhat smaller than that in a-MWNTs and the voltage range of lithiation/delithiation reaction in c-MWNTs is much wider than that in a-MWNTs. These results suggest that the chemical etching process of MWNTs makes the operating voltage of nanotubes higher (especially below 0.5 V vs. Li/Li^+) and voltage window wider.

The long-term cycling stability for c-MWNTs was practically equal to that of a-MWNTs, as shown in Fig. 5. About 87% of the initial capacity was retained after 20 cycles for both a-MWNTs and c-MWNTs. It is noted that more than half of the total capacity loss occurred for the first five cycles. After the first five cycles, the average rates of capacity fade of a-MWNTs and c-MWNTs were 0.35%/cycle and 0.40%/cycle, respectively, up to the 20th cycle.

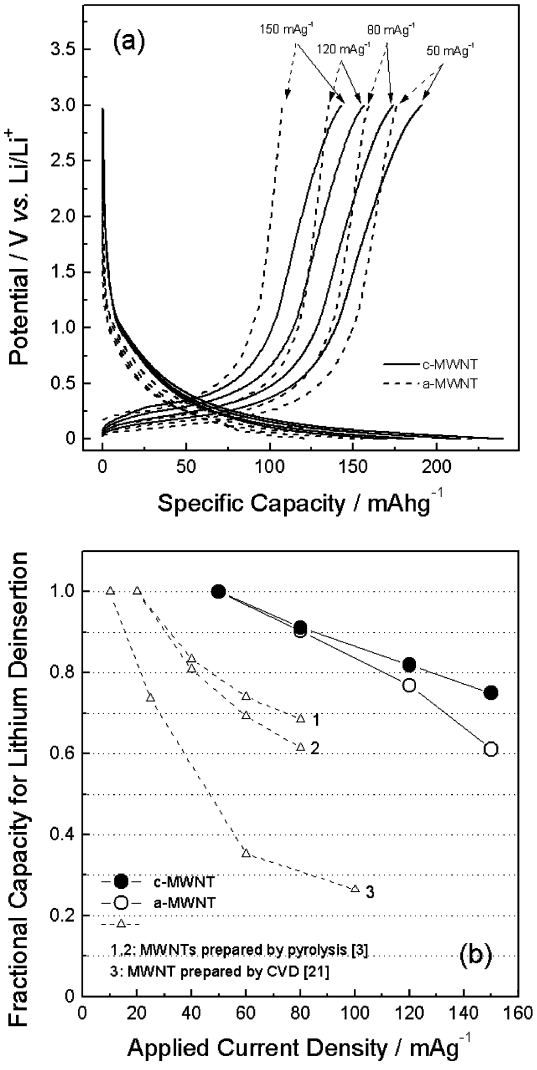

Fig. 6 (**a**) Voltage profiles obtained from a-MWNTs (*dashed lines*) and c-MWNTs (*solid lines*) in a 1 M $LiPF_6$-EC/DEC solution at different applied current densities. (**b**) The variations of fractional capacity for lithium deinsertion with applied current density, reconstructed from (**a**)

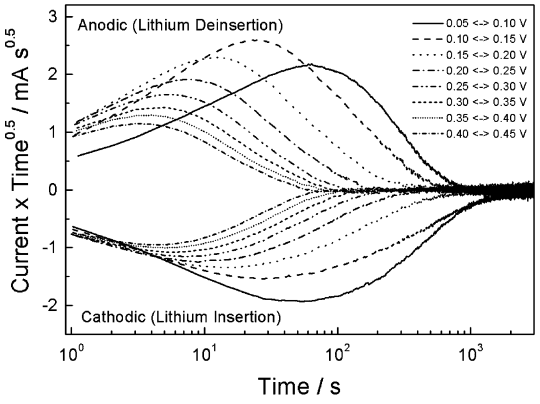

Fig. 7 Typical chronoamperometric curves obtained from c-MWNTs in a 1 M $LiPF_6$-EC/DEC solution at different potential ranges

Kinetics of lithium transport: rate capability

Shown in Fig. 6a and Fig. 6b are the voltage profiles of a-MWNTs (dotted lines) and c-MWNTs (solid lines) obtained at different current densities (50, 80, 120, and 150 mA g^{-1}) and the plots of fractional specific capacity versus applied current density, respectively. At a lithium deinsertion rate of 150 mA g^{-1}, c-MWNTs showed about 75% of capacity retention, which is ~15% higher than that for a-MWNTs. The observed rate capability of the present c-MWNTs represents the highest ever reported for MWNTs [3, 23], as seen in Fig. 6b and Table 1.

In order to explore the kinetics of lithium transport through the MWNTs, chronoamperometry was performed between 0.05 and 0.45 V (vs. Li/Li^+). Shown in Fig. 7 are the $It^{1/2}$ versus log t plots for the c-MWNTs. It is noted that there is no plateau region (i.e. no Cottrell region) throughout the lithium insertion/deinsertion time, indicating that the overall process was not controlled by lithium diffusion [24]. This further implies that the lithium transport through the c-MWNT electrode is possibly controlled by a slow interfacial reaction during the chronoamperometric measurements [24, 25]. Shown in Fig. 8a and Fig. 8b are the variation of current density and cumulative charge density with lithium insertion time, respectively, obtained for both a-MWNTs and c-MWNTs. Clearly, the lithium insertion rate (i.e. current density) into the c-MWNTs is much higher than the lithium insertion rate into the a-MWNTs. Thus, the cumulative charge densities of the c-MWNTs reached steady-state values much faster than the a-MWNTs. These results strongly indicate that the lithium transport through the c-MWNTs is much more facile than that through the a-MWNTs.

Figure 9 depicts the typical impedance spectra of a-MWNTs (open triangles) and c-MWNTs (open circles) at an electrode potential of 0.1 V (vs. Li/Li^+). It is noted that the interfacial resistance of c-MWNTs is much smaller than that of a-MWNTs. This supports the above arguments that the chemical etching of the carbon nanotubes facilitates the lithium insertion/deinsertion reaction into/from the nanotubes.

Based upon the experimental results, the observed higher rate capability of c-MWNTs than a-MWNTs can be explained as follows. First, the chemical etching process chops the tubes into short fragmented nanotubes with open ends. The shortening of the nanotubes would reduce the lithium diffusion length while the opening of the nanotube ends would provide additional active sites for lithium insertion. Second, the energetic sonication during the chemical etching would introduce lots of structural defects, especially on the outer walls of the nanotubes, further increasing the electrochemically active area for lithium insertion and further reducing the lithium diffusion length through the nanotubes. These effects mean a higher lithiation/delithiation rate up to a specific value of depth of discharge (DOD) or state of charge (SOC).

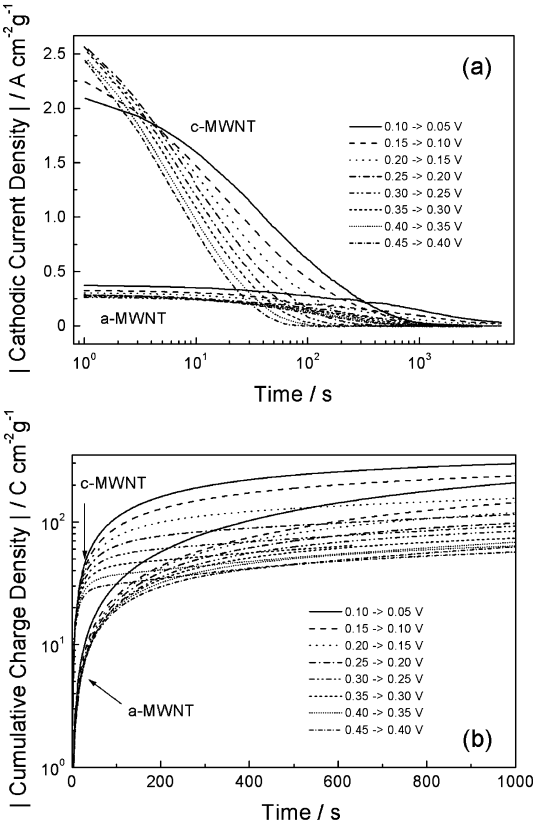

Fig. 8 (**a**) Cathodic chronoamperometric curves obtained from a-MWNTs and c-MWNTs; (**b**) the corresponding cumulative charge densities versus time

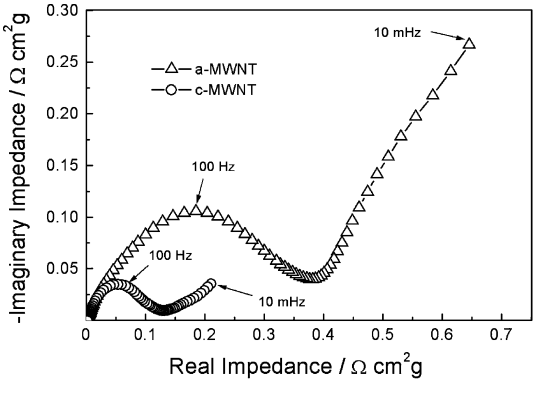

Fig. 9 Typical impedance spectra for cells with a configuration of Li|1 M $LiPF_6$-EC/DEC|MWNT (a-MWNT and c-MWNT), measured at an electrode potential of 0.1 V (vs. Li/Li^+)

Conclusions

The chemically etched (shortened) multi-walled carbon nanotubes (c-MWNTs) show a higher rate capability and reversible capacity as compared to unchopped nanotubes (a-MWNTs). Especially, the higher rate capability of c-MWNTs is attributed to a shortened lithium diffusion length through the nanotubes and an increased electrochemically active area for lithium insertion/deinsertion. However, the large irreversible capacity must be further reduced while the reversible capacity should be further improved in order to be used as an electrode material in practical lithium batteries.

Acknowledgements This work was supported by the Office of Science, Department of Energy, under grant no. DE-FG02-01ER15220. The authors are grateful to Dr Jian Dong for his HRTEM observations of the nanotubes. One of the authors (H.C.S.) would also like to acknowledge the partial support by the Post-doctoral Fellowship Program of the Korea Science & Engineering Foundation (KOSEF). A.M.R. acknowledges support for this work from a grant through the NSF grant 0132573 and ERC-NSF award no. EEC-9731680.

References

1. Frackowiak E, Gautier S, Gaucher H, Bonnamy S, Beguin F (1999) Carbon 37:61
2. Gao B, Kleinhammes A, Tang XP, Bower C, Fleming L, Wu Y, Zhou O (1999) Chem Phys Lett 307:153
3. Wu GT, Wang CS, Zhang XB, Yang HS, Qi ZF, He PM, Li WZ (1999) J Electrochem Soc 146:1696
4. Gao B, Bower C, Lorentzen JD, Fleming L, Kleinhammes A, Tang XP, McNeil LE, Wu Y, Zhou O (2000) Chem Phys Lett 327:69
5. Claye AS, Fischer JE, Huffman CB, Rinzler AG, Smalley RE (2000) J Electrochem Soc 147:2845
6. Claye AS, Fischer JE (2000) Mol Cryst Liq Cryst 340:743
7. Mukhopadhyay I, Hoshino N, Kawasaki S, Okino F, Hsu WK, Touhara H (2002) J Electrochem Soc 149:A39
8. Shimoda H, Gao B, Tang XP, Kleinhammes A, Fleming L, Wu Y, Zhou O (2002) Physica B 323:133
9. Shimoda H, Gao B, Tang XP, Kleinhammes A, Fleming L, Wu Y, Zhou O (2002) Phys Rev Lett 88:015502
10. Wang Q, Li H, Chen L, Huang X, Zhong D, Wang E (2003) J Electrochem Soc 150:A1281
11. Yang Z, Li Z, Wu H, Simard B (2003) Mater Lett 57:3160
12. Andrews R, Jacques D, Rao AM, Derbyshire F, Qian D, Fan X, Dickey EC, Chen J (1999) Chem Phys Lett 303:467
13. Shin HC, Liu M, Sadanadan B, Rao AM (2002) J Power Sources 112:216
14. Maurin G, Bousquet Ch, Henn F, Bernier P, Almairac R, Simon B (1999) Chem Phys Lett 312:14
15. Kar T, Pattanayak J, Scheiner S (2001) J Phys Chem A 105:10397
16. Meunier V, Kephart J, Roland C, Bernholc J (2002) Phys Rev Lett 88:075506
17. Lu KL, Lago RN, Chen YK, Green MLH, Harris PJF, Tsang SC (1996) Carbon 34:814
18. Aurbach D, Ein-Eli Y (1995) J Electrochem Soc 142:1746
19. Matsumura Y, Wang S, Mondori J (1995) J Electrochem Soc 142:2914
20. Flandrois S, Simon B (1999) Carbon 37:165
21. Winter M, Besenhard JO, Spahr ME, Novak P (1998) Adv Mater 10:725
22. Ong TS, Yang H (2002) J Electrochem Soc 149:A1
23. Wang GX, Ahn JH, Yao J, Lindsay M, Liu HK, Dou SX (2003) J Power Sources 119:16
24. Montella C (2002) J Electroanal Chem 518:61
25. Shin HC, Pyun SI (2002) Mechanisms of lithium transport through transition metal oxides and carbonaceous materials. In: White RE, Conway BE, Vayenas CG (eds) Modern aspects of electrochemistry, vol. 36. Plenum Press, New York, pp 255–301
26. Herstedt M, Fransson L, Edstrom K (2003) J Power Sources 124:191